*Exploration Geophysics (2004) **35**, 80–87*
Butsuri-Tansa (Vol. 57, No. 1)
Mulli-Tamsa (Vol. 7, No. 1)

Borehole radar survey to explore limestone cavities for the construction of a highway bridge

Jung-Ho Kim[1] Seong-Jun Cho Myeong-Jong Yi

Key Words: borehole radar survey, limestone cavity, anisotropy

ABSTRACT

During excavation work for the construction of a highway bridge in a limestone area in Korea, several cavities were found, and construction work was stopped temporarily. Cavities under the bridge piers might seriously threaten the safety of the planned bridge, because they could lead to excessive subsidence and differential settlement of the pier foundations. In order to establish a method for reinforcement of the pier foundations, borehole radar reflection and tomography surveys were carried out, to locate cavities under the planned pier locations and to determine their sizes where they exist.

Since travel time data from the crosshole radar survey showed anisotropy, we applied an anisotropic tomography inversion algorithm assuming heterogeneous elliptic anisotropy, in order to reconstruct three kinds of tomograms: tomograms of maximum and minimum velocities, and of the direction of the symmetry axis. The distribution of maximum velocity matched core logging results better than that of the minimum velocity. The degree of anisotropy, defined by the normalized difference between maximum and minimum velocities, was helpful in deciding whether an anomalous zone in a tomogram was a cavity or not. By careful examination of borehole radar reflection and tomography images, the spatial distributions of cavities were delineated, and most of them were interpreted as being filled with clay and/or water.

All the interpretation results implied that two faults imaged clearly by a DC resistivity survey were among the most important factors controlling the groundwater movement in the survey area, and therefore were closely related to the development of cavities. The method of reinforcement of the pier foundations was based on the interpretation results, and the results were confirmed when construction work was resumed.

INTRODUCTION

Several cavities were found by excavation work for a planned highway bridge in a limestone area in Korea, and construction work was temporarily stopped for more than one year. A serious concern for the safety of the planned bridge led us to conduct an integrated geophysical investigation, including DC resistivity, Ground Penetrating Radar (GPR), borehole radar reflection, and radar tomography surveys. The purpose of the investigation was to delineate possible cavities and weak zones, and to provide basic information for establishing the method of reinforcement of the bridge foundations. The borehole radar method played the most important role, because we believed that it could image possible cavities within the basement rock with the highest resolution among the applied methods. Construction work was stopped at the end of 1996, and we performed field work during the first half of 1997. This survey is regarded as the first attempt in Korea at the systematic application of geophysical methods to the investigation of cavities in a limestone area for construction work. Motivated by this example, it has become common practice in Korea to carry out detailed and systematic geophysical investigations before construction of large structures in limestone areas (Kim et al., 1999; Yi et al., 2002).

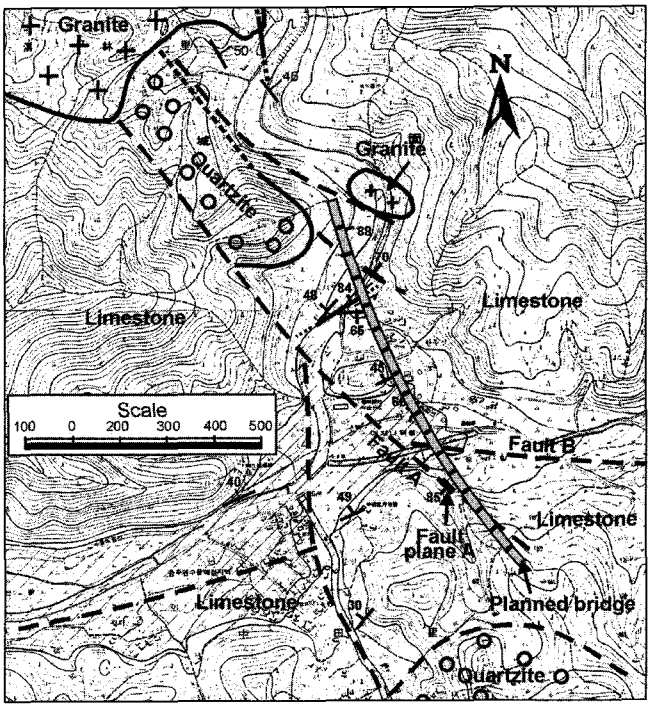

Fig. 1. Geology in the region of the planned bridge. The locations of the piers are denoted as short thick lines.

Rather than discussing all of the survey results in this paper, we have focussed our discussion on the results obtained in an area where the possibility of cavity development was expected to be highest because of the greater groundwater recharge area. Through this case history, we want to show that the borehole radar methods are good tools for the location of cavities in limestone, and furthermore, that anisotropy characteristics, when they are observed, can provide important information for understanding the internal status of the basement rock.

GEOLOGY

The geology of the survey area consists mainly of Paleozoic limestone, and Paleozoic quartzite and Jurassic granite are found in several places (Figure 1). Thin-bedded limestone is distributed under the bridge site, intercalated with calcareous shale. We can divide the survey area into two parts having different strike

Korea Institute of Geoscience and Mineral Resources (KIGAM), 30 Gaeong-dong, Yuseong-gu, Daejeon 305-350, Korea

[1] *Email: jungho@kigam.re.kr*

Manuscript received 22 July, 2003.
Revised manuscript received 12 October, 2003

directions, by an inferred fault which forms the north-eastern boundary of the quartzite in the northern part in Figure 1. Bedding planes in the south-western part show northeast strike, while those in the north-eastern part strike northwest. The most dominant fault in the survey area is Fault A, shown in Figures 1 and 2, which has been developed not by a single event but by several repeated tectonic movements, and intrusions of acidic dykes. Fault A therefore forms a fault zone consisting of fault breccia and clay, as shown in Figure 2. Another inferred fault, Fault B in Figure 1, was estimated to intersect Fault A near Pier 6 of the planned bridge. Near the intersection point of two faults, the basement would become much weaker, and many cavities might develop along the north-eastern side of Fault A, where fault breccia and clay were believed to block groundwater movement.

FIELD SURVEY AND DATA PROCESSING

Since the bridge piers, whose height is more than 50 m, are most important to the safety of the bridge, we applied borehole radar surveys to investigate the basement rock under the piers (Figure 3). For radar tomography, boreholes were drilled at both ends of each pier, and a borehole reflection survey was also conducted in all the boreholes. The average distance between two boreholes at each pier was about 25 m. The purpose of the borehole reflection survey was to detect cavities and fractures, while tomography was applied to determine the distribution of cavities and weak zones directly beneath each pier. A 20 MHz antenna was selected to overcome the severe attenuation of radar waves in this environment. Even though we used this relatively low frequency, at two piers, Pier 5 and Pier 6, it was impossible to receive transmitted radar waves, so another borehole was drilled at the centre of the line connecting the holes to get tomographic images beneath these two piers. A RAMAC Borehole system made by Mala Geoscience was used for the borehole radar surveys.

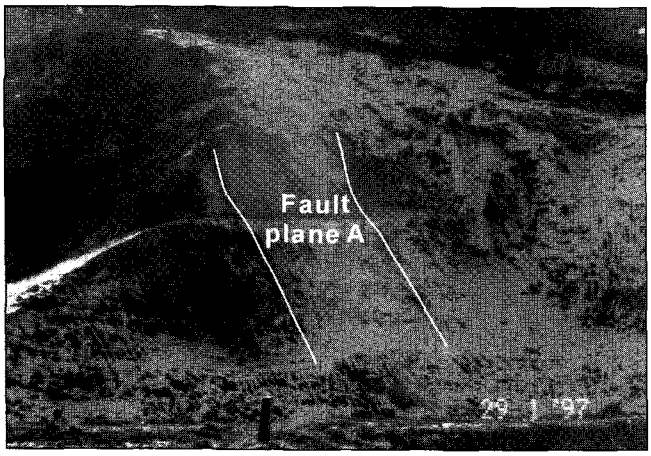

Fig. 2. The fault plane of Fault A in Figure 1, as revealed by excavation work for the construction of the foundation of Pier 5.

Velocity tomograms were constructed using first-arrival times. DC filtering was the only signal-processing scheme applied to the time series data prior to picking first-arrival times. The signals received at Pier 5 and Pier 6, however, showed very low signal-to-noise (S/N) ratio, although the distance between transmitting and receiving boreholes was about half of the separation at other piers. Therefore, before picking first-arrival times, wide-band filtering in the frequency domain was applied to the data from Pier 5 and Pier 6 to enhance the S/N ratio.

Because anisotropy phenomena were found in the first arrival times measured at six piers (Piers 5, 6, 7, 8, 10, and 14), an anisotropy-capable tomography inversion algorithm has been used to image these data sets. As borehole deviation could distort the resultant tomogram seriously (Peterson, 2001), we measured borehole deviations, using a survey instrument made by OWL Company, and corrected the picked arrival-time data for deviation effects. The tomograms corrected for deviation effects were however similar to the uncorrected ones, except those for Piers 5 and 6.

We conducted GPR and DC resistivity surveys at the surface. The GPR survey was to investigate shallow cavities, and to understand the distribution of basement rock. A RAMAC GPR system made by Mala Geoscience was used, and we acquired two data sets per survey line, one with 50 MHz and one with 100 MHz antennas.

"RADPRO for Windows", developed by the authors, was used to edit, to process, and to visualize both the GPR data and the borehole reflection data. The signal processing schemes applied involve dewowing, gain recovery, band-pass filtering in the frequency domain, predictive deconvolution, normal-move-out correction, migration, trace editing, and so on. Band-pass filtering in the spatial domain was applied to data showing severe ringing phenomena, and interactive velocity filtering or f–k domain filtering was applied where necessary.

Using a dipole-dipole array with 10-metre dipole spacing, a DC resistivity survey was conducted to delineate basement structures, including faults or fractures, and to locate possible shallow cavity zones. When we started fieldwork, many construction-work structures, such as temporary buildings, excavations, paved roads, and so on, had been constructed, so we could not avoid using

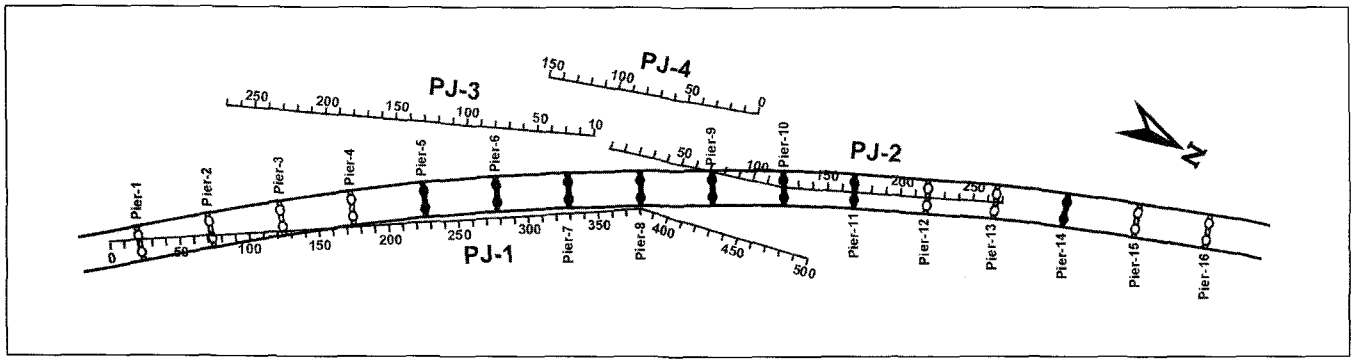

Fig. 3. Profile lines for the DC resistivity survey, and bridge piers where basement rock was investigated by the borehole radar survey. Measurement interval for the resistivity survey was 10 m, and the measurement point numbers measure distance in metres. Borehole radar surveys were carried out at the piers with filled black symbols.

crooked survey lines, or dividing one survey line into two segments, as shown in Figure 3. Field data were acquired using a Sting R1 system, made by AGI. All of the data were processed and interpreted using a 2.5D inversion scheme. "DIPRO for Windows", the 2.5D resistivity interpretation software developed by the authors, was used throughout the whole procedure of interpretation, from data editing through inversion to the reconstruction of the subsurface image.

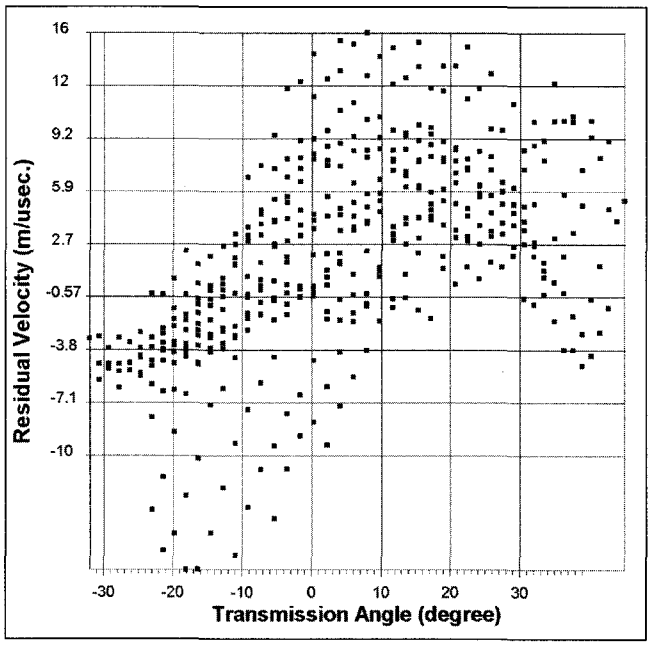

Fig. 4. A plot of residual velocity versus ray angle for radar tomography data measured between two boreholes at Pier 7. This plot clearly shows that velocity depends on the transmission angle of the radar waves.

ANISOTROPY

In some data we observed velocity anisotropy—velocity that varies depending on propagation direction. The travel-time data acquired at Piers 5, 6, 7, and 8 showed very strong anisotropy effects, and those at Piers 10 and 14 showed relatively weaker effects. In Figure 4, we demonstrate the dependence of velocity on transmission angle in the tomographic section at Pier 7. The horizontal and vertical axes represent ray angle from the source to the receiver, and residual velocity, respectively. A transmission angle of zero means that the ray propagates horizontally, i.e., the source and receiver are at the same depth level, while negative and positive values represent upward and downward propagation, respectively. Residual velocity is calculated by subtracting the average velocity on the tomographic section from the apparent velocity obtained by dividing the distance from the source to the receiver by the first arrival time. As shown in Figure 4, the velocity of a downward propagating ray is higher than that of an upward ray. As described earlier in the geology section, the main rock type in the survey area is a thin-bedded limestone with very fine bedding. We concluded that the anisotropy might result from the thin, parallel bedding planes, if the EM wave propagates faster in the direction of the bedding planes.

Figure 5a, an alternative display of the data shown in Figure 4, shows that the travel time data acquired at Pier 7 can be approximately represented by an ellipse, and the basement rock under Pier 7 can be described as a heterogeneous elliptic anisotropic medium in which the symmetry axis is not parallel to the surface. Based on this observation, we have used the anisotropic tomography algorithm developed by Jung and Kim (1999) to process the data sets which show anisotropic features in the radar velocity data. As illustrated in Figure 5b, the algorithm is based on the fact that the subsurface medium can be approximated by a heterogeneous elliptic anisotropic medium, which consists of many elliptic anisotropic cells each defined by the three material properties: maximum and minimum velocities,

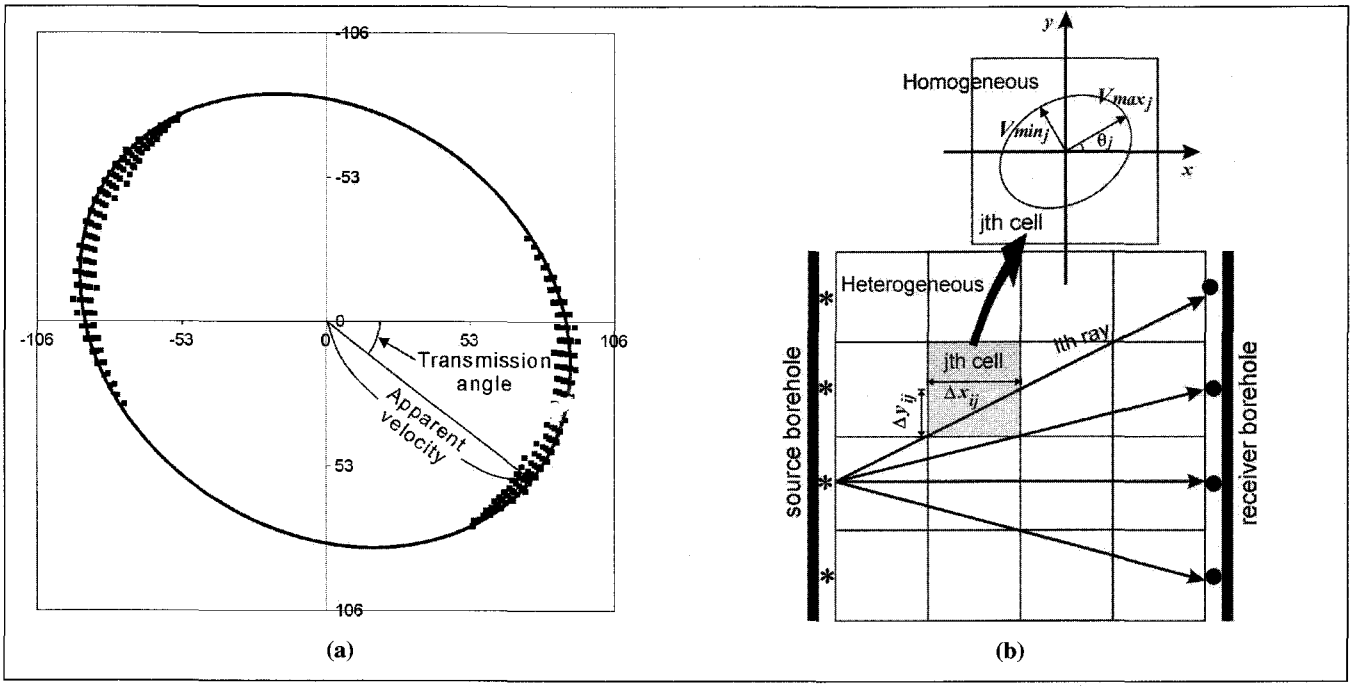

Fig. 5. (a) Polar presentation of the apparent velocity distribution for the radar tomography data measured between two boreholes at Pier 7. The distribution can be approximated by an ellipse. The radial distance of each data point from the origin is proportional to the apparent velocity, and the polar angle corresponds to the ray angle. (b) A schematic diagram showing the principle of the anisotropy tomography algorithm developed by Jung and Kim (1999).

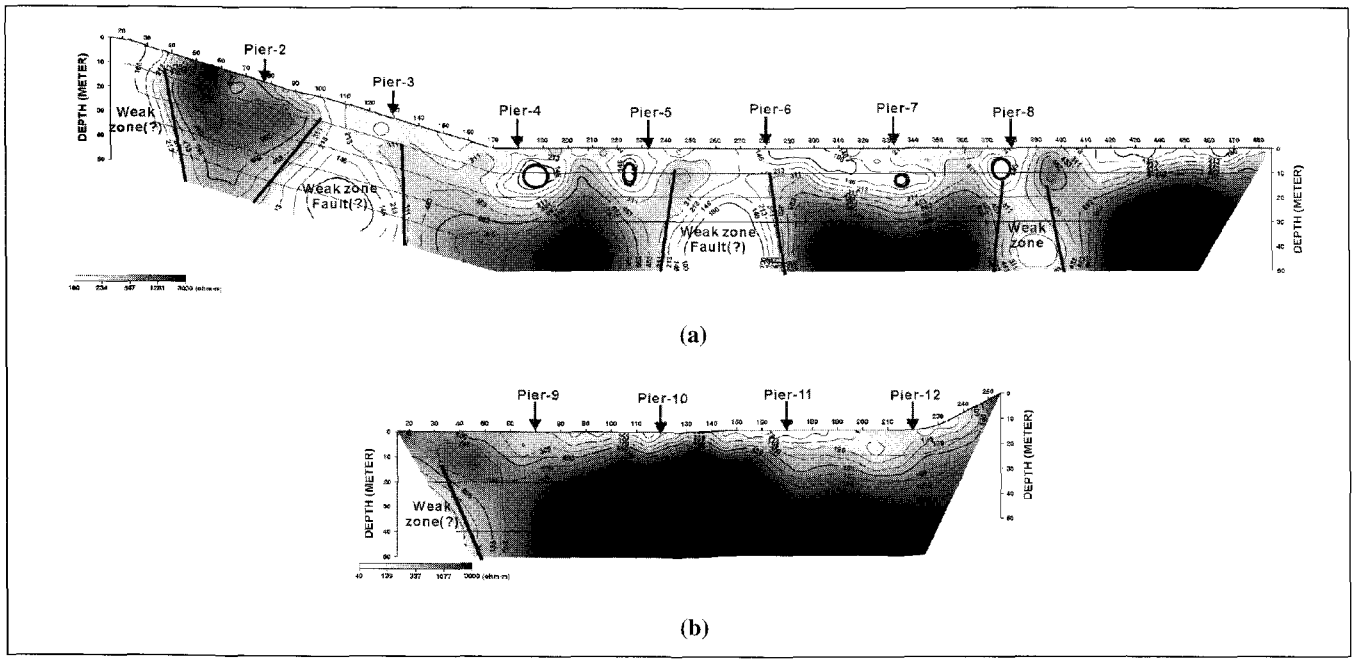

Fig. 6. Subsurface images of the resistivity survey lines PJ-1 (a) and PJ-2 (b). The measurement points nearest to bridge piers are indicated by arrows.

and symmetry axis direction. Thus, the final inverted results can be visualized with three kinds of tomograms: maximum and minimum velocities, and the direction of maximum velocity.

RESULTS OF THE DC RESISTIVITY SURVEY

An empty cavity will be imaged as a high resistivity anomaly in a DC resistivity image, while a cavity filled with clay and/or water will appear as a low resistivity anomaly. It will be relatively more difficult to identify empty cavities in resistivity images, because most limestone cavities will develop in basement rock which is relatively resistive, and so will be imaged as higher resistivity anomalies in a resistive background. On the other hand, it will be relatively easier to identify filled cavities, because they will be imaged as lower resistivity anomalies in the high-resistivity background.

A layer of relatively low resistivity, up to 300 ohm.m, is observed to extend from the surface to a depth of about 25 m (Figure 6). This could be interpreted as a soil layer, or weathered or weak basement. According to drilling results, the average depth of basement rock was only about 5–8 m, and cavities detected by drilling were filled mostly with clay. Therefore, the low resistivity layer from 10 to 25 m depth is not a soil layer, but weathered or fractured basement rock that can act as a good pathway for groundwater movement, and in which cavities are liable to develop. Within most weathered rock, it would be very unlikely that isolated anomalies with very low resistivity, such as those indicated by circles in Figure 6, would develop. Therefore, we concluded that isolated anomaly denoted by circles in Figure 6 would be cavities, or aggregates of small cavities, filled with clay and/or water. This interpretation was supported by the drilling results, which showed that most weak zones or cavities were detected in the 5–25 m depth range.

Another interesting feature in Figure 6 is that vertical anomalies with low resistivity are developed at depth, between Piers 2 and 3, between Piers 5 and 6, and near Pier 8. In particular, the vertical anomaly between Pier 2 and Pier 3 is on the extension of Fault A (Figure 1) as estimated by geological mapping. Thus, we could interpret this anomaly as Fault A. Also, the vertical anomaly between Pier 5 and Pier 6 is on the extension of Fault B (Figure 1), so we could interpret it as associated with Fault B.

Fault fractures may be good paths for groundwater, and limestone cavities are more likely to develop within them than elsewhere. Even a fault which is filled with impermeable materials, such as clay, will control groundwater movement in its vicinity. Consequently, a fault may be one of the most important factors controlling groundwater movement, and accordingly controlling the generation of limestone cavities. From this point of view, we can understand why many isolated anomalies are found near Fault A and Fault B, as shown in Figure 6a, and the frequency of isolated anomalies becomes lower with distance from these two faults (Figure 6b). We conclude that the two faults play an important role in controlling the evolution of cavities in this area.

RESULTS OF THE BOREHOLE RADAR SURVEY

A borehole was drilled at each end of every pier, for radar tomography and reflection surveys. For convenience, we label the borehole located at the east end of a pier as "R", and at the west end as "L". For example, P8-L means the borehole drilled at the western end of Pier 8. As explained above, travel time data from most piers showed anisotropy, and three kinds of anisotropic material property distributions were calculated. Because the maximum velocity tomogram turned out to be the most useful for interpretation, when compared with the available core logging results, we develop our discussion mainly from the maximum velocity tomogram. As this investigation was motivated by cavities first reported during excavation work for Pier 8, we start our discussion with the survey results at Pier 8.

As shown in the reflection images of Figure 7, the reflection data from borehole P8-L shows much higher S/N ratio than that from P8-R, and the penetration distance is longer. The same phenomena were also recognized at other piers. This observation implies that the basement under the eastern side of the bridge would be weaker than that under the western side.

In a radar reflection image, an artificially constructed cavity, such as a tunnel, will act as an ideal point reflector, and can be

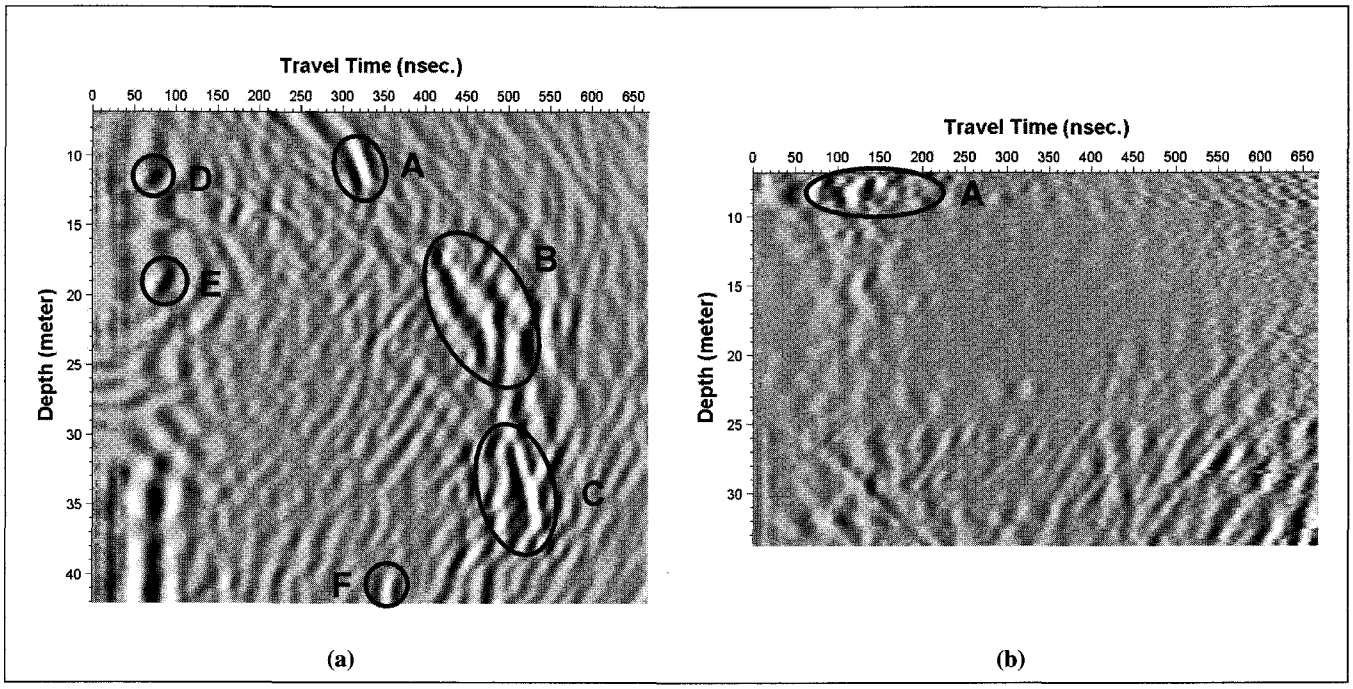

Fig. 7. Borehole radar reflection image at Pier 8. The image of P8-L (a) has been migrated, but that of P8-R (b) is unmigrated because of the very low S/N ratio.

imaged clearly as a point after migration processing. A limestone cavity, on the other hand, may not behave as a point reflector, because the shape of cavity may be irregular. Moreover, when the limestone basement contains many fracture zones caused by adjacent faults, as is the case in this area, solution cavities are usually elongated vertically, with irregular shape, by the inflow of surface water. Therefore, a cavity in limestone might be imaged as an irregular and discontinuous object from reflection data, whereas a fracture or dyke might be imaged as a relatively smoother and more continuous reflector. Because the electrical properties of the material filling the cavity, that is, air, water, or clay, are significantly different from those of the host rock, a cavity will appear as a very strong and discontinuous reflector, compared with a fracture or dyke.

This analysis implies that the three events having high reflection energy, A, B, and C, in Figure 7, would be images of cavities. We have also interpreted events D and E, showing relatively higher reflection energy, to correspond to cavities, although they are partly masked by the direct wave. In addition, event F was also interpreted to be a cavity.

Reflection energy at P8-R, the borehole at the eastern end of Pier 8, is much weaker than that at P8-L, and the penetration distance is much shorter. This could be due to the existence of a shear zone and a cavity in the depth interval 16–22 m, discovered by drilling. We can identify the reflection events from the upper and lower boundaries of the shear zone in Figure 7b. Clear reflection events could not be identified because of the influence of the shear zone, but the anomaly A was interpreted to be the response to many small-sized shallow cavities whose existence was confirmed by drilling.

On a velocity tomogram, a cavity of significant concern might be imaged as a high- or low-velocity anomaly, depending on the filling material. Most of the cavities detected during drilling for the borehole radar investigation were filled with clay, sometimes mixed with water. Therefore, our main focus was on identifying isolated low-velocity anomalies in the velocity tomogram.

In the velocity tomogram of Figure 8a, high velocities are dominant on the P8-L side, while the P8-R side shows lower velocities. In Figure 8a, green to blue colours correspond to weak rock, and in particular, the blue-coloured zone corresponds to very weak basement. The boundary between high and low velocity zones starts at the surface on the P8-L side, and becomes deeper on the P8-R side. In general, this behaviour is expected from the reflection images.

The lowest velocity appears in Zone A in Figure 8a, which represents near-surface weathered rock and an aggregation of cavities. Drilling of borehole P8-R was only completed after six attempts failed because of collapse of the boreholes, and Zone A corresponds to the depth interval where cavities were encountered in these attempts. Therefore, Zone A could be expected to be an area where many cavities would be concentrated. In addition, the isolated blue-coloured anomaly in the 18–19 m depth interval in P8-R corresponds to a cavity zone hit by drilling.

When anisotropic rock is weathered, altered, or fractured, the alignment of the direction of bedding planes, or of constituent minerals, will be diminished, so that the degree of anisotropy will become less. In the case of a cavity, because the filling material, such as air, clay, water, etc., is isotropic, the anisotropy effect will be weak where the cavity is located. This concept is supported by the observation that the degree of anisotropy in Figure 8b is very small in the uppermost part of the tomogram, corresponding to weathered rock or soil, and in all of the cavity zones detected by drilling. In Zone B in Figure 8a, represented by green colour, we can recognize some regions (Cavities 2 and 3) which show slightly low velocities but a very low degree of anisotropy, and we interpret them as cavities or cavity zones. These cavity zones are also interpreted as corresponding to the reflection events B and C in Figure 7a. We have interpreted Cavities 4 and 5 in Figure 8 to be cavities based on the appearance on the tomograms, i.e., low velocity and weak anisotropy. We have also concluded that the reflection event E in Figure 7a corresponds to Cavity 4.

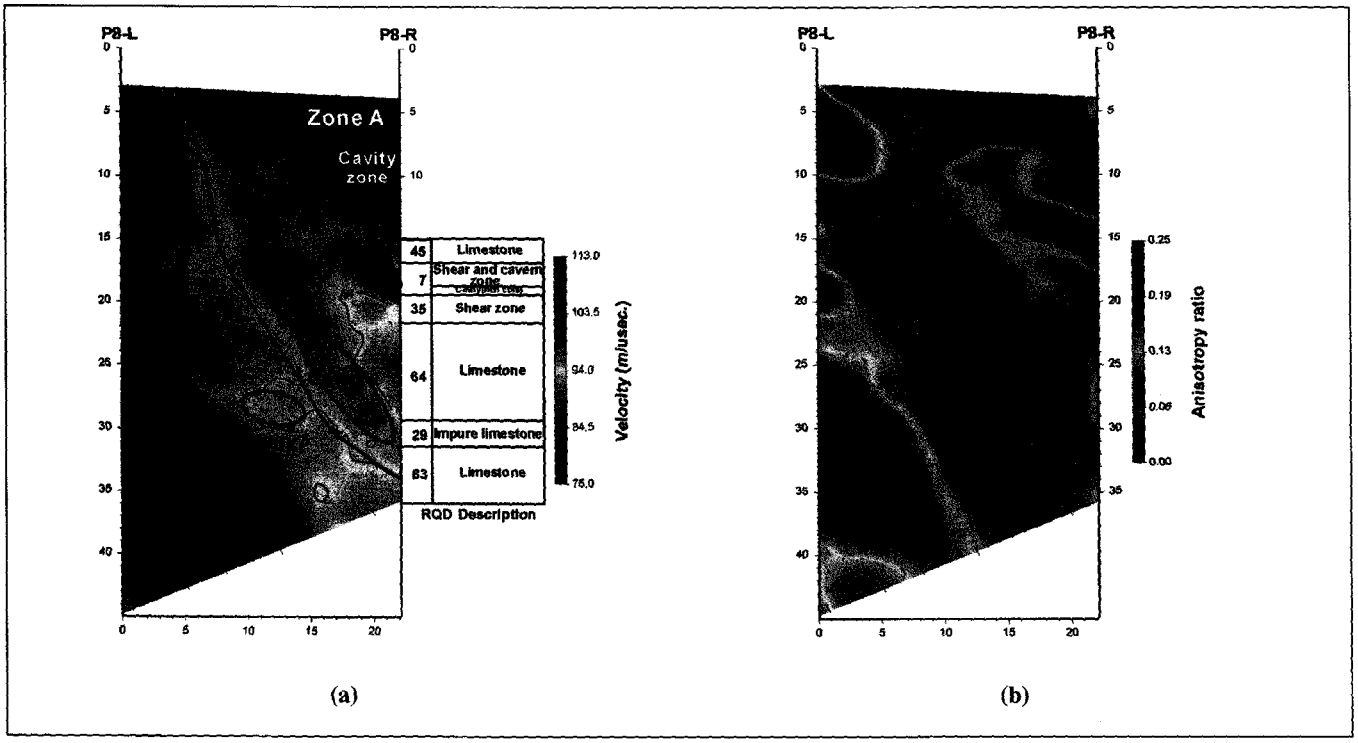

Fig. 8. Tomograms of maximum velocity (a) and degree of anisotropy (b) at Pier 8. "Degree of anisotropy" means the difference between maximum and minimum velocities, normalized by the maximum velocity. The oblique short line in a tomogram points in the direction of maximum velocity, while its length represents the degree of anisotropy. Note that the RQD attached to the borehole axis of P8-R matches fairly well with the velocity distribution.

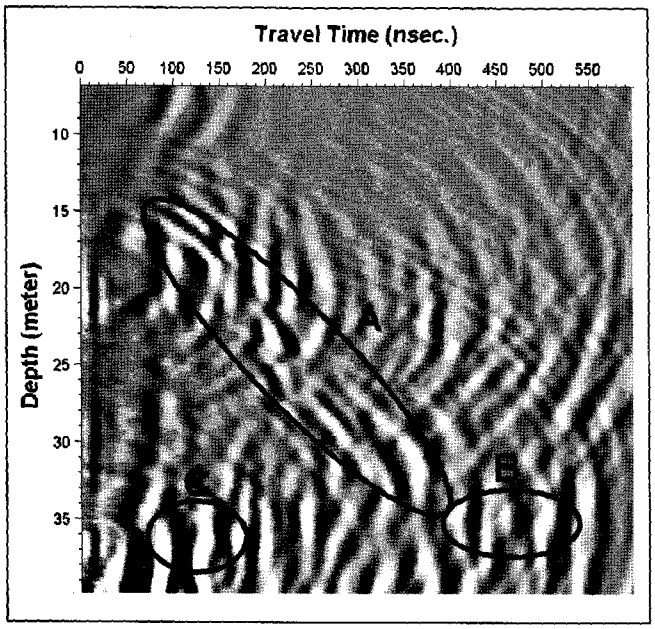

Fig. 9. Migrated image of borehole radar reflection data at borehole P7-L.

We now move our discussion to the results from Pier 7. Comparing the reflection images from boreholes P7-L (Figure 9) and P8-L (Figure 7a), located at the same western end of each pier, we can see that the penetration distance of the data acquired at P7-L is much shorter than that at P8-L, and the S/N ratio is also lower. This implies that the basement under Pier 7 is weaker than that under Pier 8, which may be due to the fact that Pier 7 is located closer to Fault B as inferred from the DC resistivity survey and geological mapping. We recognize several strong reflection events, marked as A in Figure 9, which have been interpreted to be cavities. As these reflections appear to be aligned to some extent, we have concluded that the inferred cavities are developed along a bedding plane. Anomaly B also has been interpreted to be a cavity that appears to be an extension of A.

As in the case of Pier 8, the velocity tomogram of Figure 10a shows that the eastern basement under Pier 7 is weaker than the western one, while the average velocity is slightly lower than that under Pier 8. The lowest velocity appears in Zone A in Figure 10a, and the shape and location of the anomalies in the tomogram is very similar to the case of Pier 8 (Figure 8a). Many cavities were encountered at the depth interval of Zone A during the drilling of P7-R, and the degree of anisotropy is very weak in Zone A, as shown in Figure 10b. These observations suggest that many cavities are clustered in Zone A.

An interesting feature in Figure 10a is Zone B, aligned along the boundary of the high-velocity zone. We notice that the position and the orientation of Zone B are very similar to those of reflection events A in Figure 9. Cavities 1, 2, 3, and 4 in Figure 10a are inferred cavities based on the velocity distribution, the degree of anisotropy, and the reflection events. In particulary, we have interpreted that Cavity 1, hit during drilling of P7-R, corresponds to event B, and Cavity 4 to event C, in Figure 9.

Pier 6 is very close to Fault B inferred by the DC resistivity survey and geological mapping. It was almost impossible to receive any radar signals during the acquisition of tomography data because of the severe attenuation of EM waves caused by the very low resistivity of the fault zone. Therefore, we drilled another borehole, P6-C, at the centre of a line connecting the other two boreholes, and constructed a complete tomographic image beneath Pier 6 by performing two tomography surveys: between P6-L and P6-C, and between P6-C and P6-R. Although the distance between transmitting and receiving boreholes was about half of that at other piers, the S/N ratio in the tomography data was quite low. Because of this low S/N ratio, we could pick first-arrival

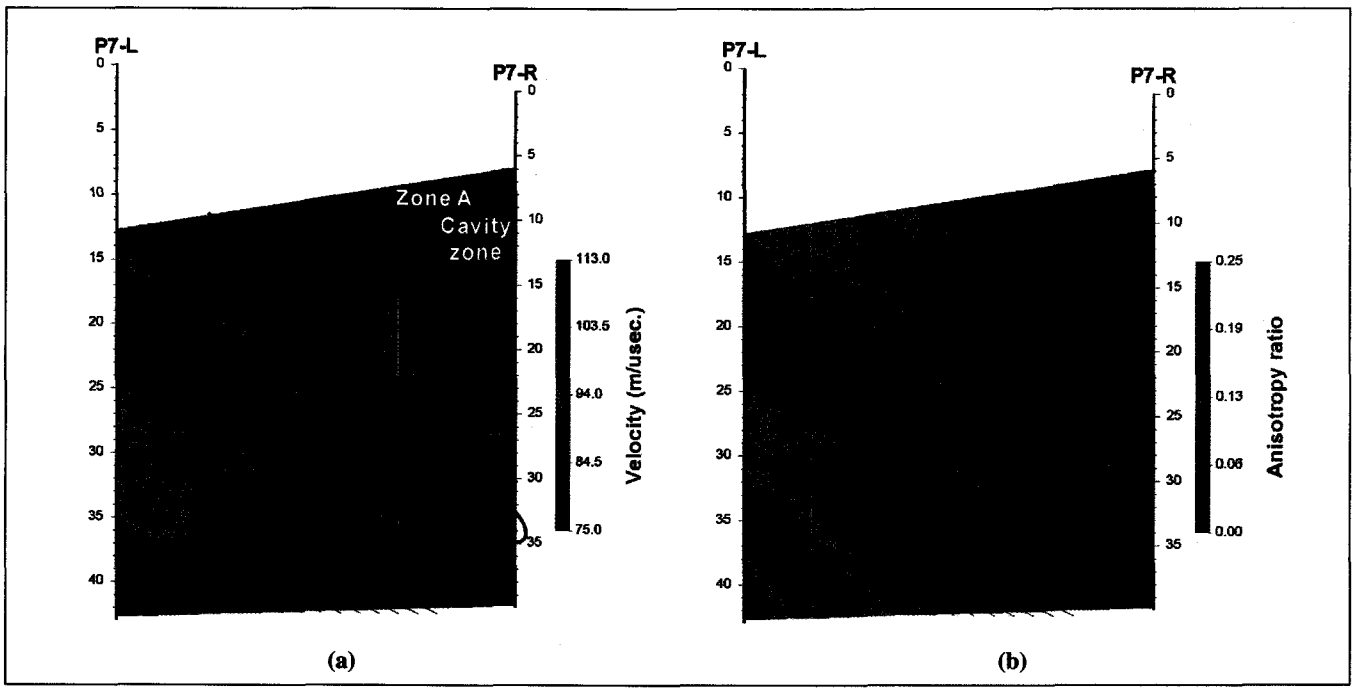

Fig. 10. Tomograms of maximum velocity (a) and degree of anisotropy (b) at Pier 7.

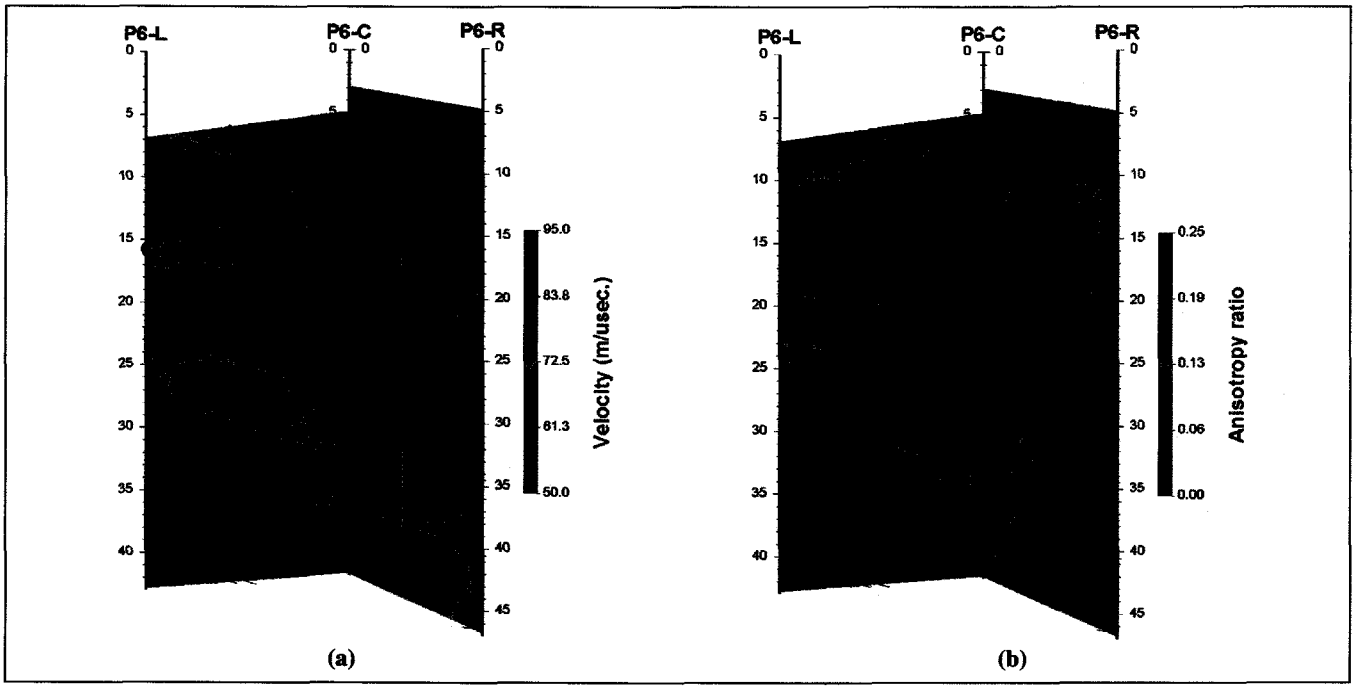

Fig. 11. Tomograms of maximum velocity (a) and degree of anisotropy (b) at Pier 6.

times only after applying band-pass filtering. We also attempted borehole reflection surveys in all three boreholes, but we could not get meaningful reflection images because of the very severe signal attenuation.

In general, the velocity distribution in Figure 11a shows reasonable continuity at the boundary between the two adjacent tomograms. The direction of maximum velocity, however, shows some discrepancy at the junction between the two sections. This discrepancy is mainly due to a very low S/N ratio in the tomography data, compared with that at other piers, and to the fact that the direction of symmetry axis has the lowest sensitivity among the three variables in anisotropic inversion. The EM wave velocities in Figure 11a are much lower than those at other piers, except Pier 5 (see Figure 12), and the maximum velocity tomogram overall shows that the velocity is lower than 80 m/μsec except in the lower-left corner. This image suggests that the whole section below Pier 6 should be regarded as a weak zone. We have also compared RQD (Rock Quality Designation) values available at the borehole P6-L with the velocity distribution near the borehole. The results show that the green- and blue-coloured area in the figure is a very weak zone, and that even the red colour corresponds to altered or soft rock.

The inferred cavities, or cavity zones, marked in Figure 11a, are zones of low velocity and low degree of anisotropy. This interpretation was based on the evidence that cavities were met during drilling of boreholes P6-L and P6-C at depths of about

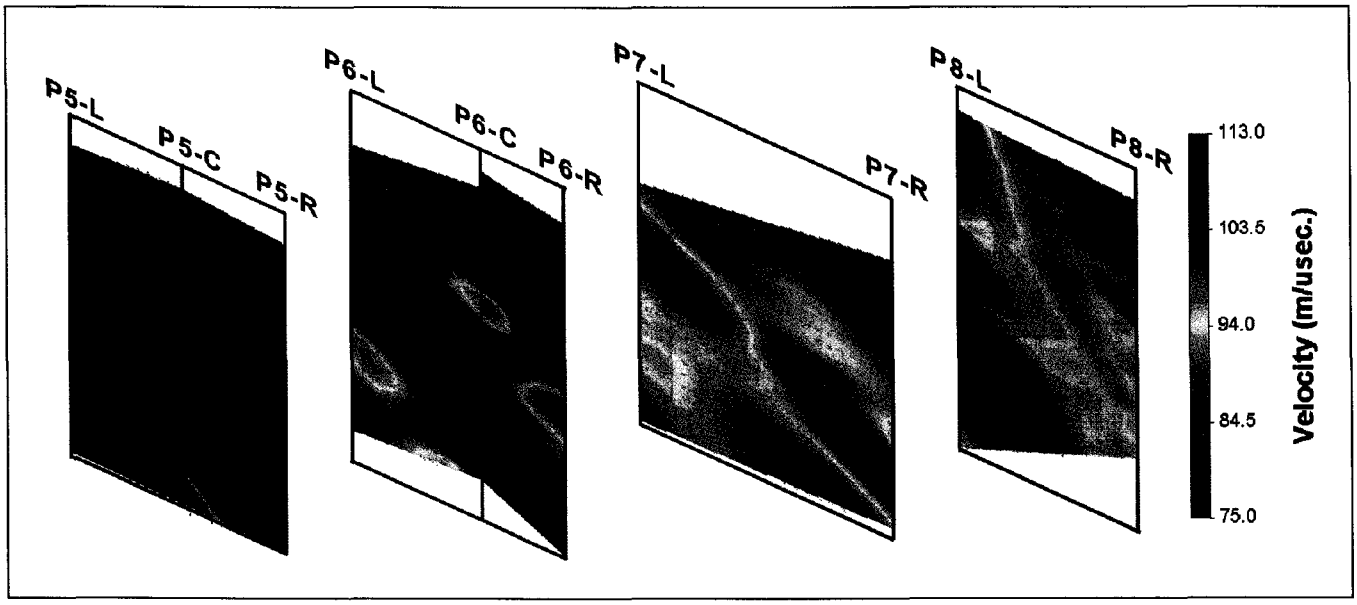

Fig. 12. Comparative display of the maximum velocity tomograms beneath Piers 5, 6, 7, and 8.

16 m and 40 m, respectively. Our interpretation is once more substantiated by the fact that both radar velocity and degree of anisotropy show quite low values in these regions.

DISCUSSION AND CONCLUSIONS

Figure 12 illustrates the maximum velocity tomograms under four adjacent piers, with the same velocity scale, for the purpose of comparison. As we move to Pier 5 from Pier 8, the blue colour becomes dominant, that is, the average velocity becomes lower. This implies that the basement rock becomes weaker and the influence of Faults A and B becomes greater. Moreover, the frequency of occurrence of cavities increases going from Pier 8 to Pier 5. These facts suggest that Faults A and B are among the most important factors controlling groundwater flow, and thus, the formation of cavities in this area.

Figure 12 also shows an interesting feature in that the weak zone extends more deeply under the eastern part of each pier than under the western part. Moreover, as discussed in the previous section, the frequency of occurrence of cavities in the eastern part is higher than in the western part. If this feature were not considered in the construction of the bridge, it will be highly likely for the bridge to suffer excessive subsidence and, furthermore, differential settlement, because the eastern alignment of the bridge would be placed on a very poor foundation, whereas the western one would be on a relatively better foundation.

From the viewpoint of foundation stability, Pier 6 was predicted to be the most unstable. Although the average velocity of the radar wave is least at Pier 5, the velocities at Pier 6 are comparable to Pier 5, and the frequency of occurrence of cavities at Pier 6 is much higher than that of Pier 5. Considering all the investigation results; geological mapping, surface geophysics, borehole radar, and drilling results, we have concluded that weakness of the pier foundations would decrease in the following order: Piers 6, 5, 7, 8, 9, 10, and 11.

The results discussed so far have led us to the conclusion that borehole radar methods are good tools for the location of cavities in limestone areas. One of the greatest advantages of borehole radar methods is that we can get images not only of material properties, through radar tomography, but also of boundaries of inhomogeneities, through reflection surveys. We have confirmed that the anisotropic characteristic itself gives us very important information. When the subsurface material is anisotropic, the degree of anisotropy, defined by the normalized difference between maximum and minimum velocities, is helpful in interpreting whether or not an anomalous zone in a radar tomogram is a cavity. In addition to detailed surveying with borehole radar, it is useful to conduct a surface DC resistivity survey, if possible, not only to get information on the subsurface distribution of resistivity, but also to find the detailed geological structure, which is useful in the interpretation of borehole radar surveys.

ACKNOWLEDGEMENT

This work was partly supported by the Korean Ministry of Science and Technology, through a National Research Laboratory (NRL) project under contract No. 2000-N-NL-01-C-113.

REFERENCES

Jung, Y., and Kim, J.-H., 1999, Application of anisotropic georadar tomography to monitor rock physical property changes: *Journal of Environmental and Engineering Geophysics*, **4**, 87–92.

Kim, J.-H., Cho, S.-J., Yi, M.-J., Song, Y., and Chung, S.-H., 1999, Application of borehole radar survey to detect cavities in limestone area: *Proceedings of the Symposium on the investigation of limestone cavities and abandoned tunnels, and reinforcement method*, 93–118 (in Korean), Korean Geotechnical Society.

Peterson, J. E. Jr., 2001, Pre-inversion corrections and analysis of radar tomographic data: *Journal of Environmental and Engineering Geophysics*, **6**, 1–18.

Yi, M.-J., Kim, J.-H., Song, Y., Chung, S.-H., 2002, Application of three-dimensional resistivity imaging technique to the site investigations, *Symposium on the Application of Geophysics to Engineering and Environmental Problems (SAGEEP 2002)*, Las Vegas, 13IDA10.